# Cold Pool and Precipitation Responses to Aerosol Loading: Modulation by Dry Layers

LEAH D. GRANT AND SUSAN C. VAN DEN HEEVER

*Colorado State University, Fort Collins, Colorado*

(Manuscript received 9 September 2014, in final form 16 December 2014)

ABSTRACT

The relative sensitivity of midlatitude deep convective precipitation to aerosols and midlevel dry layers has been investigated in this study using high-resolution cloud-resolving model simulations. Nine simulations, including combinations of three moisture profiles and three aerosol number concentration profiles, were performed. Because of the veering wind profile of the initial sounding, the convection splits into a left-moving storm that is multicellular in nature and a right-moving storm, a supercell, which are analyzed separately.

The results demonstrate that while changes to the moisture profile always induce larger changes in precipitation than do variations in aerosol concentrations, multicells are sensitive to aerosol perturbations whereas supercells are less so. The multicellular precipitation sensitivity arises through aerosol impacts on the cold pool forcing. It is shown that the altitude of the dry layer influences whether cold pools are stronger or weaker and hence whether precipitation increases or decreases with increasing aerosol concentrations. When the dry-layer altitude is located near cloud base, cloud droplet evaporation rates and hence latent cooling rates are greater with higher aerosol loading, which results in stronger low-level downdrafts and cold pools. However, when the dry-layer altitude is located higher above cloud base, the low-level downdrafts and cold pools are weaker with higher aerosol loading because of reduced raindrop evaporation rates. The changes to the cold pool strength initiate positive feedbacks that further modify the cold pool strength and subsequent precipitation totals. Aerosol impacts on deep convection are therefore found to be modulated by the altitude of the dry layer and to vary inversely with the storm organization.

## 1. Introduction

Aerosol–cloud interactions have received much attention over the past few decades by virtue of their potential to influence important aspects of the Earth–atmosphere system, including precipitation and radiation. However, characterizing aerosol impacts on deep convection has remained challenging, in part because of highly nonlinear microphysical–dynamical feedbacks, as summarized by Tao et al. (2012).

Several studies have found that aerosols can invigorate deep convective cloud updrafts through enhanced latent heating associated with freezing (Andreae et al. 2004; Khain et al. 2005; van den Heever et al. 2006). Other more recent modeling and observational studies have shown that enhanced aerosol concentrations lead to fewer, larger raindrops in warm-phase (Altaratz et al. 2008; Berg et al. 2008; Saleeby et al. 2010) and convective clouds (Storer et al. 2010; May et al. 2011; Lim et al. 2011; Khain et al. 2011; Storer and van den Heever 2013; Loftus and Cotton 2014). These studies attribute the larger raindrops to greater rain accretion rates due to higher cloud water contents in polluted clouds compared with clean clouds, as well as to the shedding and melting of larger hailstones. The populations of larger raindrops fall faster and also have less net surface area, which reduces evaporative cooling rates in the downdraft, and hence weakens the cold pool and subsequent dynamical forcing (van den Heever and Cotton 2007; Storer et al. 2010; Morrison 2012).

The importance of environmental parameters such as relative humidity, vertical wind shear, and instability in regulating aerosol impacts on deep convection and associated precipitation totals has also been previously highlighted. For instance, Khain et al. (2008) found that precipitation associated with deep convection increased with increasing aerosol concentrations for high humidity but decreased for low humidity because of enhanced hydrometeor evaporation. Cui et al. (2011) demonstrated that the development of a single convective

*Corresponding author address:* Leah D. Grant, Colorado State University, 1371 Campus Delivery, Fort Collins, CO 80523.
E-mail: ldgrant@atmos.colostate.edu

DOI: 10.1175/JAS-D-14-0260.1

cloud was more strongly impacted by aerosol loading when a midlevel dry layer was present compared to conditions with higher midlevel humidity. Storer et al. (2010) found that aerosol impacts on deep convection were greater for lower convective available potential energy (CAPE), which indicates that the ability of aerosols to influence deep convective precipitation depends on the strength of the dynamical forcing and, by extension, the storm organization. This was also suggested by Seifert and Beheng (2006), who found that supercell storm characteristics, including total precipitation and updraft strength, are less sensitive to aerosols than are multicells.

Although multiple studies have investigated aerosol impacts on deep convection under different environmental humidity profiles (e.g., Khain et al. 2005; Tao et al. 2007; Khain et al. 2008; Lee 2011; Cui et al. 2011), none of these have investigated the importance of the vertical location of the dryness. Yet, the altitude of dry layers has previously been shown to play an important role in accumulated convective precipitation, cloud-top height, cold pool characteristics, and storm morphology (Brown and Zhang 1997; Gilmore and Wicker 1998; Ridout 2002; Grant and van den Heever 2014, hereafter GvdH14). The goal of this study is therefore to investigate the relative influence of midlevel dry layers and aerosols on both multicellular and supercellular deep convective precipitation. It will be demonstrated that the less-organized multicellular convection is more sensitive to aerosols than are the more organized supercells. The multicell precipitation sensitivity arises through feedbacks on the strength of the cold pool. Such feedbacks are shown to depend on the altitude of the dry layer above cloud base.

## 2. Methods

Idealized cloud-resolving model simulations have been performed with version 6 of the Regional Atmospheric Modeling System (RAMS) (Cotton et al. 2003; Saleeby and van den Heever 2013). RAMS contains a sophisticated two-moment bulk microphysics scheme that predicts supersaturation as well as mixing ratio and number concentration for eight hydrometeor types, including cloud, drizzle, rain, pristine ice, snow, aggregates, graupel, and hail (Walko et al. 1995; Meyers et al. 1997; Saleeby and Cotton 2004). The hydrometeor size distributions are represented by gamma functions; a shape parameter of 2 has been used for all species in these simulations. To emulate a bin microphysics scheme, the RAMS microphysics also utilizes lookup tables generated from offline parcel model calculations for several microphysical processes, including activation, collection, and sedimentation (e.g., Feingold and Heymsfield 1992; Saleeby and Cotton 2008).

RAMS microphysics is coupled to an advanced aerosol parameterization scheme that represents two ammonium sulfate modes, two dust modes, three sea salt modes, and two regenerated aerosol modes using a lognormal distribution (Saleeby and van den Heever 2013). For the simulations presented in this study, only the small modes of both sulfates and dust were included. The sulfate- and dust-mode median diameters were set to 0.15 and 0.1 $\mu$m and the solubility fractions were set to 0.8 and 0.05, respectively, similar to Seigel et al. (2013). Each of the two modes has a distribution spectral width of 1.8. Cloud droplet activation from the aerosol field is determined from the lookup tables based on the vertical velocity, temperature, and aerosol number concentration, median size, and solubility fraction. The largest aerosol particles in the distribution with diameters exceeding 0.5 $\mu$m nucleate ice crystals as a function of temperature, following the DeMott et al. (2010) ice nucleation parameterization. Nucleation and deposition sinks and evaporation and surface sources of aerosol were not included in these idealized simulations for simplicity so that the aerosol species were not overly depleted throughout the simulation. As such, the results described in this paper may represent the upper limit of aerosol impacts on the deep convective cloud systems studied here.

The model configuration was the same as that used in GvdH14 and is reiterated here as follows. The horizontal grid spacing was 300 m, and a 25-m vertical grid spacing near the surface was stretched vertically to a maximum of 300 m. The domain size of 285 $\times$ 225 $\times$ 22 km$^3$ included 950 $\times$ 750 $\times$ 92 grid points. The simulations were run for 3 h with a time step of 1 s. Open radiative lateral boundary conditions (Klemp and Wilhelmson 1978) and a Smagorinsky (1963) turbulent diffusion scheme were used. Surface energy fluxes and radiation responses were not included. The initial horizontally homogeneous thermodynamic and wind profiles for the control simulation (herein CTL) were adapted from the analytical sounding in Weisman and Klemp (1982) and the strongest half-circle hodograph in Weisman and Klemp (1984), respectively. Surface-based CAPE is approximately 1800 J kg$^{-1}$ in this environment. Convection was initialized with a 2-K thermal perturbation.

Dry layers are ubiquitous in midlatitude convective environments as air is advected from different source regions under directionally sheared vertical wind profiles (Carlson and Ludlam 1968), such as commonly occurs near the dryline because of advection of the elevated mixed layer, as discussed in GvdH14. Therefore, GvdH14 investigated the impacts of dry layers at three

different altitudes and of three different strengths on supercell morphology. Three of the moisture profiles investigated therein are utilized in this study: CTL (the moist profile), and two dry-layer scenarios M25 [the middle (M)-altitude, 2–3-km dry layer with a 25% reduction in water vapor] and H50 [the highest (H)-altitude, 3–4-km dry layer with a 50% reduction in water vapor], both of which had similar precipitable water reductions of 10%–12% from CTL. The characteristics of the top and bottom of the dry layers were gradually smoothed back to the original CTL moisture profile at 1 km below and 2 km above the dry layer. Therefore, although the M25 dry layer is strongest between 2 and 3 km, it fully extends from 1 to 5 km; similarly, the H50 dry layer fully extends from 2 to 6 km, as shown in Fig. 1a.

To address the goals of this study, three different aerosol number concentration profiles were tested for each of these three moisture profiles (Fig. 1b). The cleanest profile for each of the two aerosol species, which contained a surface number concentration of 100 $cm^{-3}$ that decreased linearly to 10 $cm^{-3}$ at 4 km and was held constant above 4 km, is the same as that used in all nine dry-layer simulations in GvdH14. Since this aerosol profile applies to a submicron mode of both ammonium sulfate and dust, the total aerosol number concentration is actually double that shown in Fig. 1b. In the more polluted aerosol tests, aerosol concentrations for each of the two species were multiplied everywhere by a factor of 4 and 16 so that the surface concentrations were 400 and 1600 $cm^{-3}$, respectively. The three aerosol concentration profiles were chosen to cover a wide range of relatively pristine and polluted conditions that have also been tested in previous idealized modeling studies (e.g., Ekman et al. 2007; Storer et al. 2010; Lim et al. 2011; Storer and van den Heever 2013; Loftus and Cotton 2014). Such high aerosol concentrations may occur in continental midlatitude regions as a result of anthropogenic aerosol sources and various dust source regions (e.g., Prospero et al. 2002). The simulations discussed in this paper are named by the moisture profile (CTL, M25, or H50), followed by the surface aerosol number concentration for the individual aerosol type (100, 400, or 1600).

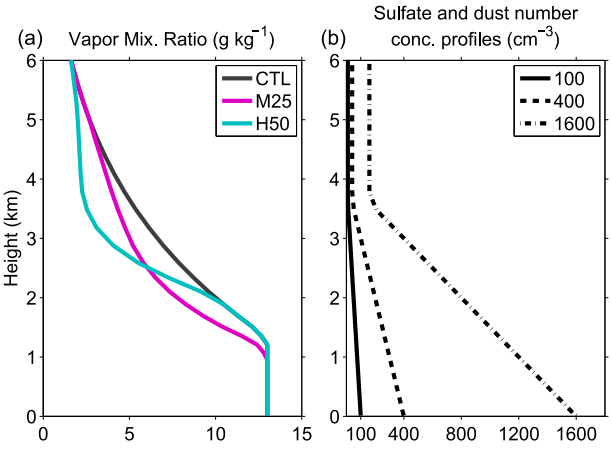


FIG. 1. (a) Initial water vapor mixing ratio for the three moisture profiles, after GvdH14. (b) Initial aerosol number concentration profile for both ammonium sulfate and dust modes for the aerosol sensitivity experiments. Note that the total aerosol number concentrations are therefore double that shown here. The labels in the legend refer to the number concentrations at the surface.

## 3. Impacts on precipitation

Because of the veering wind profile, the initial convection in each simulation splits into a left-moving storm (the multicellular storm) and a right-moving storm (a supercell) (Fig. 2). To separately analyze the multicell and supercell storms and their relative sensitivity to aerosols and midlevel dryness, the domain was subjectively divided such that the accumulated precipitation exceeding 1 mm for the supercell was located in the southern portion and the multicellular precipitation was contained in the northern portion. The results presented in this paper are insensitive to 10-km shifts of this subjective division to the north or south, since the analysis focuses on the latter half of the simulations in order to avoid the influence of the initial conditions. At these times, the supercell and multicell storms are also more widely separated. The domain divisions for CTL-100, CTL-1600, M25-100, and M25-1600 are indicated in Fig. 2.

Several important points are qualitatively evident in the accumulated precipitation and vertically integrated condensate fields shown in Fig. 2. First, the supercell characteristics and precipitation show substantial sensitivity to the vertical moisture profile [in fact, the M25 right movers are low-precipitation supercells (Figs. 2c,d), as demonstrated in GvdH14] but very little sensitivity to aerosols. Second, the multicellular structure and precipitation resulting from the initial left mover are also strongly impacted by the dry layer. However, the multicell storms are clearly sensitive to aerosol loading as well. For instance, the number of convective cells and accumulated multicellular precipitation notably increases from M25-100 to M25-1600 (Figs. 2c,d).

The response of the accumulated precipitation to changing aerosol concentrations for the entire domain, only the supercell, and only the multicells under all three moisture profiles is quantified in Fig. 3. It is clear that the presence of the dry layer has a much stronger influence on the accumulated precipitation than do variations in aerosol concentrations. The largest

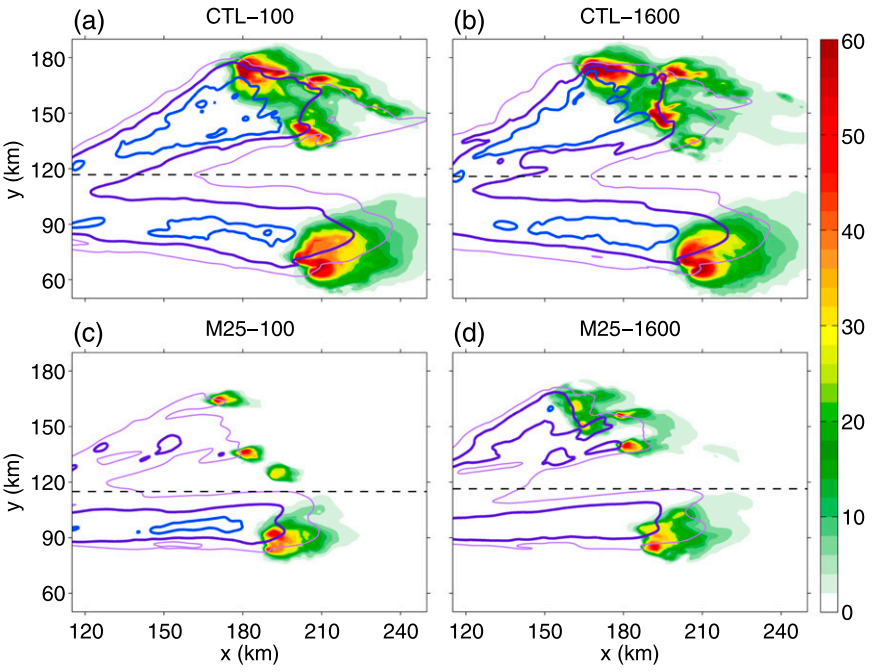


FIG. 2. Vertically integrated condensate (shaded, mm), accumulated precipitation [contours at 1 (light purple), 5 (purple), and 15 (blue) mm], and domain divisions for the supercell and multicells (black dashed line) in simulations (a) CTL-100, (b) CTL-1600, (c) M25-100, and (d) M25-1600 at 160 min.

reduction in the full-domain accumulated precipitation relative to CTL-100 is about 70% for M25-100, whereas the largest change due to increased aerosol concentrations occurs between H50-100 and H50-1600 and is only a 16% reduction.

Separating the accumulated precipitation into the contributions from the multicells and supercells reveals additional interesting trends. The accumulated precipitation from the supercell is reduced for all three moisture profiles by about 15% when aerosol concentrations are increased from the moderately polluted (400) to the most polluted (1600) conditions, which is also qualitatively evident in Fig. 2. Previous studies of aerosol influences on supercells have also found decreasing trends in precipitation with increasing aerosol concentrations, although in a few instances the supercell precipitation increased for different environments (e.g., relative humidity) or microphysical schemes (Seifert and Beheng 2006; Khain and Lynn 2009; Storer et al. 2010; Lim et al. 2011; Morrison 2012). However, a substantially different pattern emerges for the multicellular precipitation. While enhanced aerosol concentrations make very little difference in the multicellular precipitation for the CTL moisture profile, the precipitation increases in M25 by about a factor of 2 but decreases by 16% in H50 between the cleanest and most polluted cases. This result demonstrates several important points: 1) the mechanism by which aerosols influence deep convective precipitation appears to be different for supercells and multicells; 2) the magnitude, and even the sign, of aerosol impacts on multicellular precipitation is sensitive to the vertical distribution of moisture.

Aerosol impacts on supercells and multicells are different by virtue of the differences in storm dynamics associated with these storm types. Supercells are highly organized and strongly dynamically forced through vertical perturbation pressure gradients resulting from the rotating updraft and its interaction with the environmental shear (Rotunno and Klemp 1982; Davies-Jones 2002). Supercell updraft rotation arises through the vertical tilting of horizontal vorticity that is associated with the environmental wind shear (e.g., Droegemeier et al. 1993). As such, aerosols do not substantially impact the supercellular strength and resulting precipitation. On the other hand, the low-level cold pool forcing plays a significant role in the development and maintenance of the multicell storm, and hence it may be susceptible to aerosol-induced changes in the cold pool strength. Therefore, the cold pool responses to varying aerosol concentrations and the processes responsible for the multicellular precipitation trends noted above are next investigated.

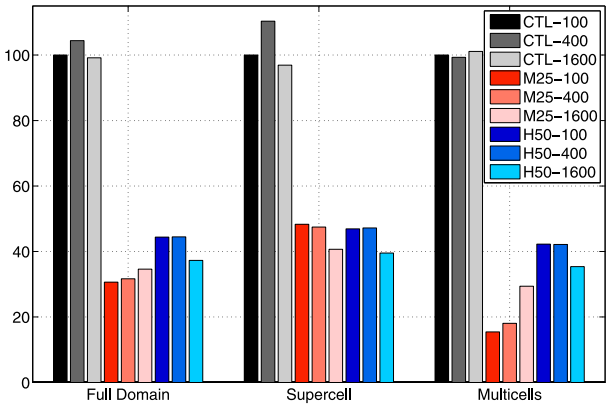


FIG. 3. Total accumulated precipitation after 3 h, expressed as a percentage of CTL-100, for the entire domain, for the southern portion containing the supercell, and for the northern portion containing the multicells.

## 4. Cold pool feedbacks in multicells

The same trends in multicellular precipitation as noted above—namely, that precipitation increases for the M25 moisture profile but decreases for the H50 profile with increasing aerosol concentrations, are evident in the time series of total precipitation rate produced by the multicells (Fig. 4a). However, it can be seen that the precipitation rates for the aerosol experiments in M25 and H50 do not begin to deviate significantly from their respective clean simulations until 120–150 min into the simulation.

It is widely accepted that multicellular convection is dynamically forced by lift associated with convergence at the cold pool's leading edge (e.g., Thorpe and Miller 1978; Thorpe et al. 1982; Fovell and Tan 1998; Lin et al. 1998). Recent studies have suggested that feedbacks to the cold pool and rainfall are possible with these types of convective systems (van den Heever and Cotton 2007; Tao et al. 2007; Lee et al. 2008; Storer et al. 2010; Morrison 2012; Seigel et al. 2013). For example, if a factor—such as aerosol loading—causes cold pools to become colder, the cold pool lift is strengthened, which can enhance subsequent convection and rainfall. Greater rainfall production further strengthens the cold pool by evaporative cooling, which represents a positive feedback to the cold pool strength. Therefore, it may be expected that the trends in the cold pool temperatures will correlate with the trends in the rainfall, which is in fact qualitatively evident in Fig. 5. For instance, the multicellular cold pools for the H50 and M25 moisture profiles are warmer and smaller than those in CTL regardless of the aerosol concentration, since both H50 and M25 produce less precipitation. This result is consistent with James and Markowski (2010). Moreover, as aerosol concentrations are increased, the cold pools are colder and larger for the M25 moisture profile and warmer and smaller for the H50 moisture profile. This qualitative result is demonstrated quantitatively in the time series of the minimum density potential temperature perturbation (Emanuel 1994), which is directly related to the cold pool buoyancy (Fig. 4b). With increasing aerosol concentrations, the minimum cold pool buoyancy is more negative in M25 but less negative in H50 throughout most of the time series, which is in agreement with the precipitation trends (Fig. 3).

The changes in cold pool buoyancy with increasing aerosols are already evident at around 90 min when the multicellular storm enters the northern portion of the domain (Fig. 4b). However, significant changes in the precipitation rate do not occur until later. In particular, the precipitation rate becomes noticeably larger in M25-1600 compared to M25-100 at 120 min and substantially larger after 150 min (Fig. 4a). During this same time period, the M25-1600 cold pool buoyancy decreases even further relative to M25-100 (Fig. 4b), and the area of strong midlevel updrafts also increases by at least a factor of 2 (Fig. 4c). These time series for the M25 multicells therefore demonstrate how the initial changes in the cold pool buoyancy due to aerosols feed back to the convection and rainfall, which in turn further enhances the cold pool strength through evaporative cooling, representing a positive feedback to the rainfall. The opposite effect occurs for the H50 moisture profile; initially at around 90 min, aerosol impacts cause the cold pool negative buoyancy to weaken (Fig. 4b), which weakens the cold pool's dynamical forcing and reduces the amount of subsequent convection between 120 and 150 min (Fig. 4c).

The final piece of the puzzle then is why enhanced aerosol concentrations initially increase the cold pool negative buoyancy when the dry layer is lower but decrease the negative buoyancy when the dry layer is higher, thus initiating the respective positive feedbacks? Throughout most of the time series, the area of midlevel convective updrafts is smaller in the M25 scenarios than in the H50 scenarios, irrespective of aerosol concentrations (Fig. 4c). Previous studies have found that smaller clouds are more diluted by entrainment (e.g., Khairoutdinov and Randall 2006; Kuang and Bretherton 2006). Figure 4c therefore demonstrates that entrainment is more detrimental to the developing convection when the dry layer is lower, as previously discussed by James and Markowski (2010). Also, dry layers have a greater potential to enhance evaporatively driven downdrafts when they are lower in altitude (Gilmore and Wicker 1998). The cloud base is near 1.2 km, corresponding to the top of the

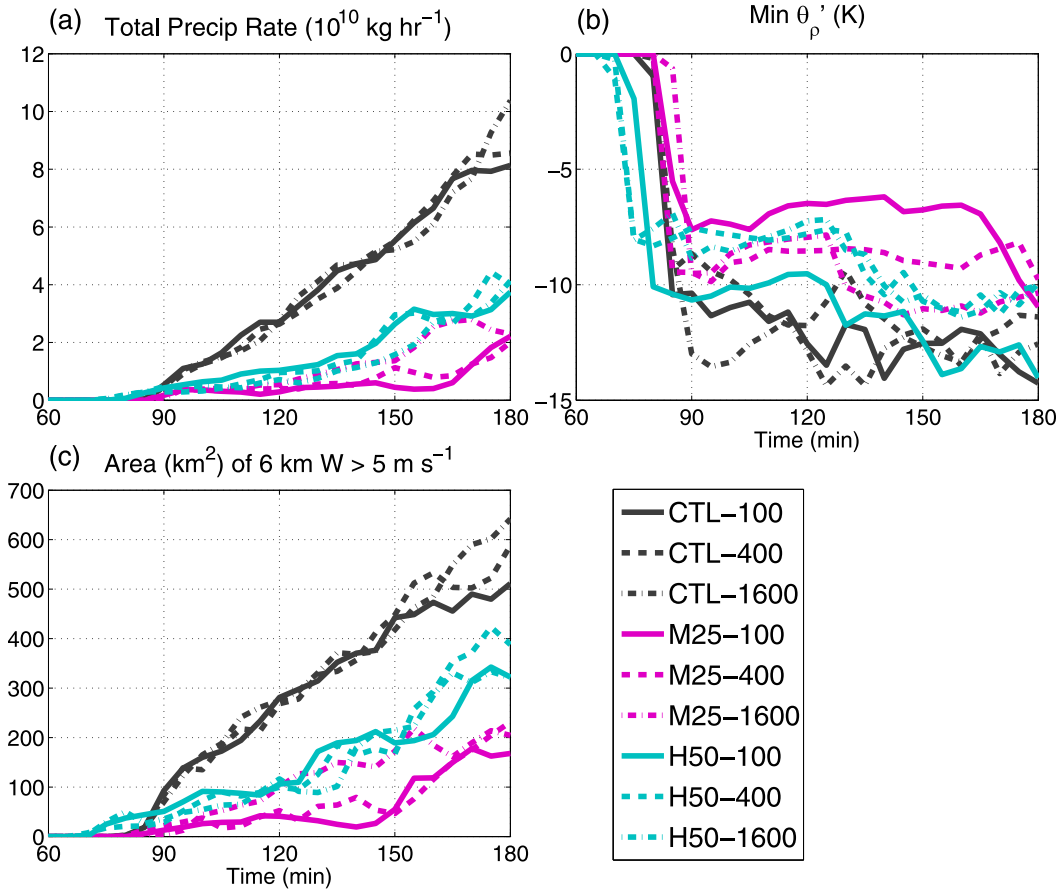


FIG. 4. Time series of (a) total precipitation rate, calculated as in GvdH14, (b) minimum density potential temperature perturbation within the lowest 100 m AGL, and (c) area of the 6-km updrafts exceeding 5 m s$^{-1}$. Results are shown for the northern portion of the domain containing the multicells.

well-mixed boundary layer (Fig. 1a), and the bottom of the M25 dry layer begins just below cloud base as described in section 2 and shown in Fig. 1a. The smaller *cloud droplets* near cloud base in the more polluted cases have a greater net surface area and hence evaporate more quickly, which strengthens the downdrafts (e.g., Khain et al. 2005; Tao et al. 2007; van den Heever and Cotton 2007; Lee et al. 2008). Therefore, the initially colder cold pool in the more polluted M25 simulations can be attributed to enhanced evaporative cooling in the downdrafts. To verify this, downdrafts with magnitudes exceeding 1 m s$^{-1}$ were averaged for the multicellular convection (Fig. 6a). The downdrafts are consistently stronger by up to 0.5 m s$^{-1}$ in the more polluted M25 simulations compared with M25-100. Furthermore, average latent cooling rates in the downdrafts increase from values of up to 2 K h$^{-1}$ in M25-100 to 5 K h$^{-1}$ in M25-1600 (not shown). This result agrees with previous findings that enhanced evaporation in the downdrafts due to smaller cloud droplets can lead to increases in the precipitation by secondary convection under certain humidity conditions (e.g., Khain et al. 2005; Tao et al. 2007; van den Heever and Cotton 2007).

When the dry layer is higher, as in H50, entrainment is less detrimental to the convection, as is evidenced by the larger updraft areas in comparison to those in M25 (Fig. 4c). Additionally, in the H50 cases, the entire dry layer is located above cloud base (Fig. 1a). Therefore, the higher altitude of the dry layer is less influential in enhancing the low-level downdrafts through cloud droplet evaporation. In this case, the changes in the low-level (in and below cloud) *raindrop* characteristics become more important than the cloud droplet characteristics in determining the downdraft and cold pool response to aerosol loading. The average raindrop number concentrations are reduced and raindrops are larger in H50 as aerosol concentrations are increased (Figs. 6c,d), which is in agreement with recent studies (Storer et al. 2010; May et al. 2011; Lim et al. 2011; Storer and van den Heever 2013). The fewer, larger

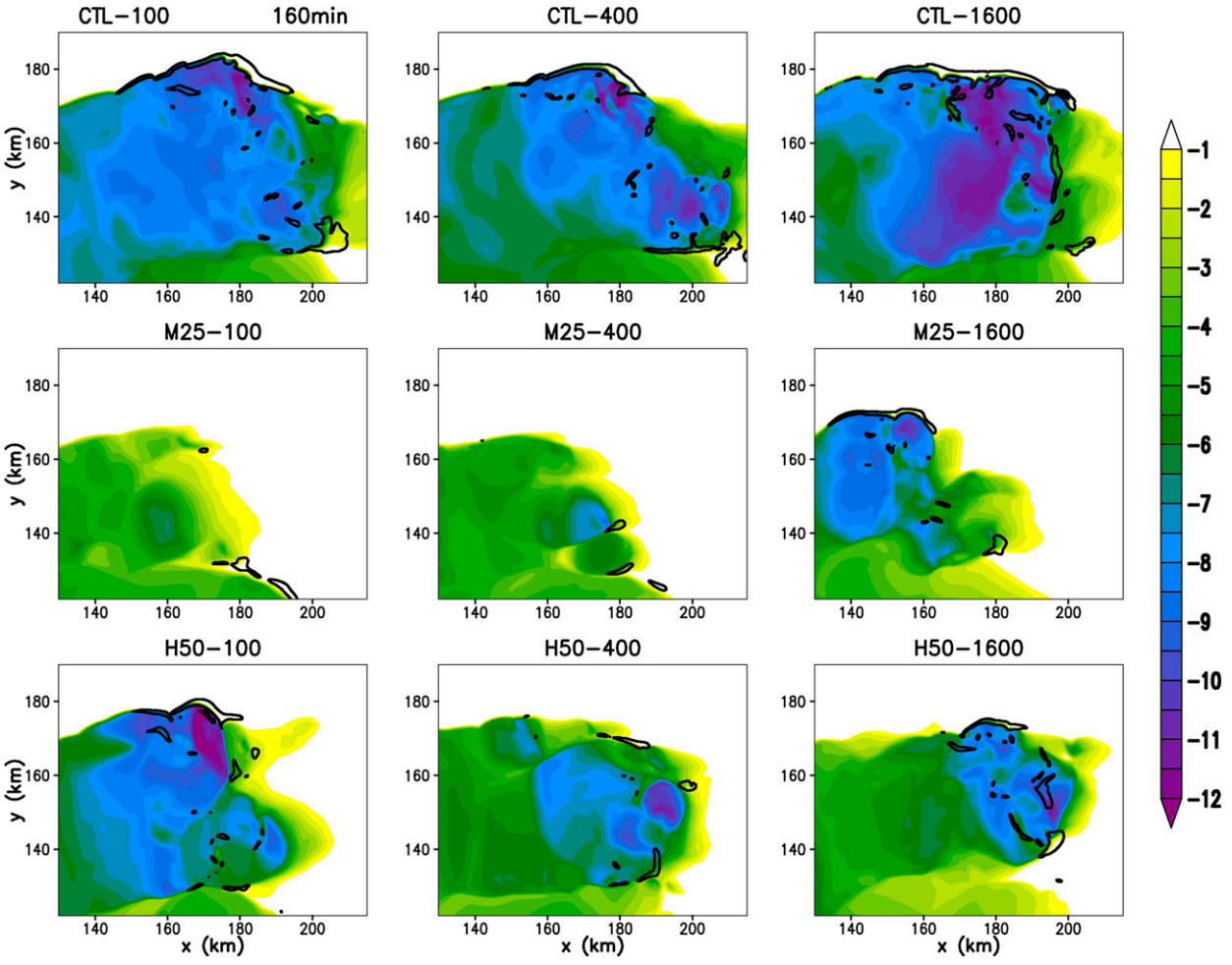


FIG. 5. Perturbation density potential temperature at the lowest model level (K, shaded) and 0.5-km-AGL convergence (0.005-$s^{-1}$ black contour) at 160 min for the (top) CTL, (middle) M25, and (bottom) H50 moisture profiles and (left) 100, (center) 400, and (right) 1600 aerosol tests. Results are demonstrated for the northern portion of the domain containing the multicells.

raindrops fall faster and have less net surface area, which reduces the average latent cooling rates in the low-level downdrafts by up to 2 K $h^{-1}$. Consequently, even though the downdrafts are stronger above about 3 km where the dry layer is centered, the downdrafts below 2 km (near and below cloud base) are weaker in the more polluted H50 simulations compared with H50-100 (Fig. 6a). The differences in the raindrop characteristics can therefore explain the initially less negatively buoyant cold pools and subsequent rainfall reductions in the polluted H50 simulations.

The cold pool feedback mechanisms discussed above have been demonstrated for the 90–150-min time period shown in Fig. 4. It is interesting to note that some of the differences between the clean and polluted simulations for the two dry-layer cases decrease toward the end of the 3-h simulation, such as can be seen in the midlevel updraft area and minimum density potential temperature perturbation time series for the M25 simulations (Figs. 4b,c). However, the overall trends in cold pool buoyancy and area demonstrated in Fig. 5 at 160 min hold true at the end of the simulation. We suspect that, given the consistent systematic differences in the cold pools with increasing aerosol concentrations for the M25 and H50 dry-layer scenarios, the differences in the time series of precipitation rate, cold pool strength, and updraft area would increase again beyond 3 h. However, longer simulations over a significantly larger domain would be necessary in order to capture the dissipating stage of these convective systems and confirm this conjecture.

Some of the previous studies investigating aerosol impacts on deep convection under different humidity profiles have shown that cold pools become colder and hence precipitation increases, while other studies have

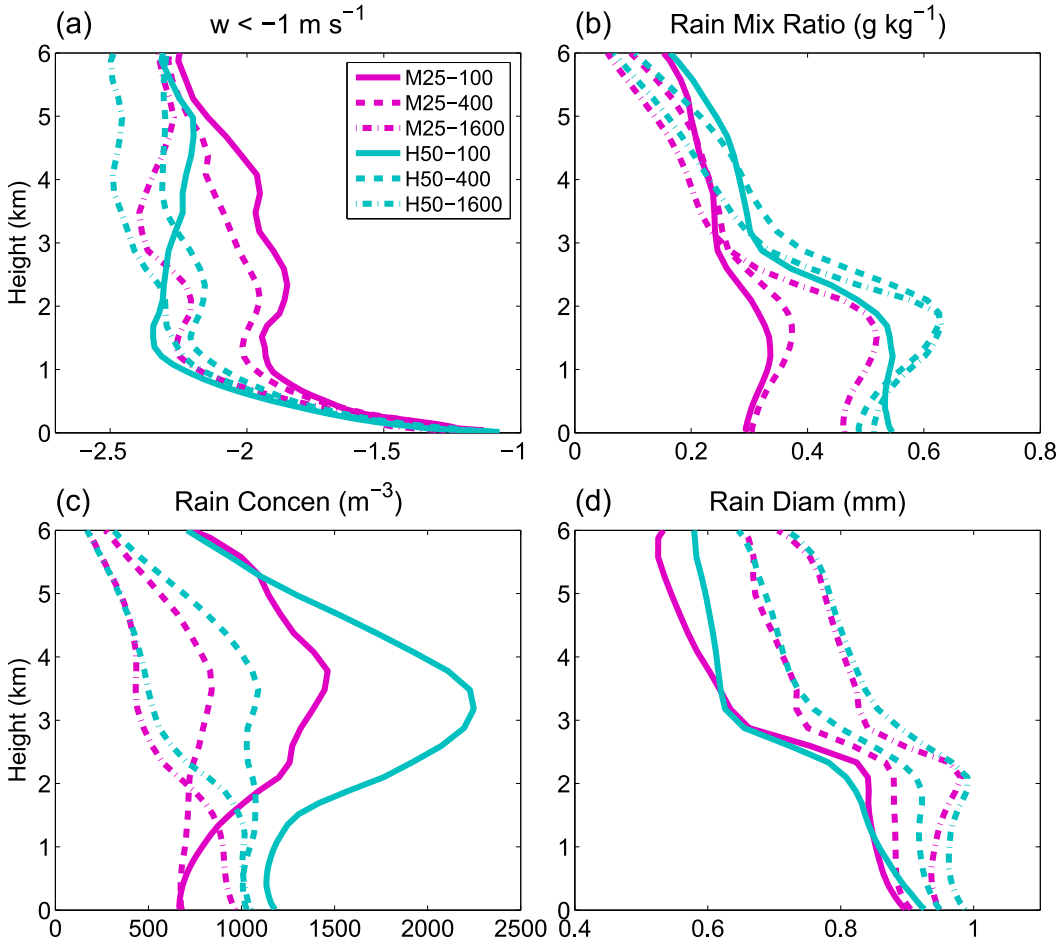


FIG. 6. (a) Downdraft strength, (b) rain mixing ratio, (c) raindrop number concentration, and (d) volume-mean rain diameter, averaged from 90 to 180 min over the northern portion of the domain containing the multicellular convection, for all the dry-layer experiments. Downdrafts are averaged only where $w < -1\,\mathrm{m\,s^{-1}}$, rain mixing ratio and number concentration are averaged only where total condensate is greater than $0.01\,\mathrm{g\,kg^{-1}}$, and rain mean diameter is averaged only where rain mixing ratio is greater than $0.01\,\mathrm{g\,kg^{-1}}$.

demonstrated that cold pools are warmer and precipitation is reduced with increasing aerosol concentrations. Based on the findings presented here, we hypothesize that the contrasting cold pool responses in these studies may be due to different vertical distributions of moisture—in particular, the dry-layer altitude relative to cloud base. For instance, Tao et al. (2007) simulated a squall line under clean and polluted conditions using a sounding taken in Kansas. In this case, the cold pools became warmer and precipitation decreased in more polluted conditions. The Kansas sounding is relatively dry only above approximately 600 hPa (Johnson and Hamilton 1988, their Fig. 8). Tao et al. noted that rain evaporation dominated at low levels, and evaporative cooling rates, while enhanced above 4 km in the polluted case, were reduced below 3 km (see their Fig. 9b). Hence the high altitude of the dryness may explain why Tao et al. found warmer cold pools with increasing aerosols, as in the H50 case shown here. Similarly, Storer et al. (2010) and Morrison (2012) both demonstrated in their simulations that cold pools were warmer under more polluted conditions. Both studies partially attributed the warmer cold pools to reduced rain evaporation resulting from fewer, larger raindrops. The relatively moist Weisman and Klemp (1982) sounding was used in both Storer et al. (2010) and Morrison (2012). Hence it is likely that enhanced cloud droplet evaporation due to entrainment was not very important in influencing the downdrafts and cold pool strength in these two studies. Conversely, Lee (2011) found that downdrafts were strengthened through increased evaporative cooling with increasing aerosol concentrations. The evaporative cooling was further enhanced under drier conditions. The initial water vapor

profile used in Lee (2011) was much drier above the boundary layer (1.6 km) than in the present study, and the moisture profile was modified by decreasing the relative humidity in the entire column above the boundary layer. Hence, as stated in that study, changes in the cloud droplet size distribution were more important than changes in the raindrop size distribution in determining the latent cooling response to increasing pollution. Therefore, these results suggest that it is the vertical moisture distribution—in particular the dry layer altitude in relation to cloud base—that is important in determining the overall cold pool sensitivity and hence precipitation response to increasing aerosol loading in multicellular convective systems.

## 5. Summary and conclusions

The goal of this study has been to investigate the *relative* sensitivity of multicells and supercells to environmental dry layers and to aerosol loading. This goal has been accomplished with idealized high-resolution simulations using the RAMS model, in which three different moisture profile and aerosol number concentration profile combinations were simultaneously varied for a total of nine simulations. The multicells and supercells were analyzed separately. For both types of convection, the influence of the dry layer always outweighed the impact of varying the aerosol concentrations. However, variations in aerosol concentrations were found to influence the convective precipitation, particularly the precipitation resulting from the multicell storms. The main findings regarding aerosol influences are summarized as follows:

- *Aerosol impacts on multicells are modulated by midlevel dry layers through feedbacks to the strength of the cold pool.* It was shown that the sign and magnitude of the multicellular precipitation response to aerosol loading depends on the vertical distribution of moisture. This dependency arises through cold pool feedbacks that begin with net changes in latent cooling rates associated with both cloud droplet and raindrop evaporation. Under more polluted conditions, cloud droplets are smaller and more numerous, while raindrops are larger and less numerous. The smaller, more numerous cloud droplets evaporate more efficiently, which enhances latent cooling rates. On the other hand, the fewer, larger raindrops fall faster and evaporate less quickly, which reduces latent cooling rates. The increase in cloud droplet evaporation rates dominates when the dry layer is located near cloud base, and therefore downdrafts are strengthened, the cold pool becomes colder, dynamical lifting along its leading edge is enhanced, and precipitation subsequently increases under more polluted conditions. However, when the dry layer is located higher above cloud base and entrainment is less detrimental to the convection, the changes to the low-level (below cloud base) raindrop evaporation rates become more important than changes in the cloud droplet evaporation rates. This results in weaker downdrafts, a warmer cold pool, and subsequently less precipitation under more polluted conditions.
- *Aerosol influences on deep convection vary inversely with the storm organization.* Among the multicell storms simulated here, the least organized storms in terms of the cold pool strength and midlevel updraft area occur with the M25 moisture profile (Fig. 4). The M25 multicell storms were also found to be the most sensitive to aerosol loading (Fig. 3). On the other hand, the CTL multicell storms are the most organized in terms of the cold pool strength and updraft area, and they are the least sensitive to aerosol loading. Moreover, supercells, which are highly organized, are the least sensitive to aerosols, while the less organized multicellular convection shows much larger sensitivities to aerosol loading, which is in agreement with previous findings (Seifert and Beheng 2006; Storer et al. 2010). This demonstrates fundamental differences in the mechanisms by which aerosols can impact precipitation in supercells and multicells by virtue of the differences in the storm dynamics, in particular the cold pool forcing, associated with these convective types.

Based on these findings, we conclude that multicells may be some of the more susceptible midlatitude convective types to aerosol perturbations and that this sensitivity depends critically on environmental conditions such as the vertical distribution of moisture. Given the importance of multicellular convective systems in contributing to midlatitude precipitation, it is important that future work focus on better characterizing their sensitivity to aerosol loading under a wide range of environmental conditions.

*Acknowledgments.* The research presented in this manuscript was made possible by a Graduate Student Fellowship from the Cooperative Institute for Research in the Atmosphere (CIRA). The authors thank three anonymous reviewers for their comments and suggestions that led to an improved manuscript. High-performance computing support from Yellowstone (ark:/85065/d7wd3xhc) was provided by NCAR's Computational and Information Systems Laboratory, sponsored by the National Science Foundation.

## REFERENCES


Altaratz, O., I. Koren, T. Reisin, A. Kostinski, G. Feingold, Z. Levin, and Y. Yin, 2008: Aerosols' influence on the interplay between condensation, evaporation and rain in warm cumulus cloud. *Atmos. Chem. Phys.,* **8,** 15–24, doi:10.5194/acp-8-15-2008.

Andreae, M. O., D. Rosenfeld, P. Artaxo, A. A. Costa, G. P. Frank, K. M. Longo, and M. A. F. Silva-Dias, 2004: Smoking rain clouds over the Amazon. *Science,* **303,** 1337–1342, doi:10.1126/science.1092779.

Berg, W., T. L'Ecuyer, and S. van den Heever, 2008: Evidence for the impact of aerosols on the onset and microphysical properties of rainfall from a combination of satellite observations and cloud-resolving model simulations. *J. Geophys. Res.,* **113,** D14S23, doi:10.1029/2007JD009649.

Brown, R. G., and C. Zhang, 1997: Variability of midtropospheric moisture and its effect on cloud-top height distribution during TOGA COARE. *J. Atmos. Sci.,* **54,** 2760–2774, doi:10.1175/1520-0469(1997)054<2760:VOMMAI>2.0.CO;2.

Carlson, T. N., and F. H. Ludlam, 1968: Conditions for the occurrence of severe local storms. *Tellus,* **20,** 203–226, doi:10.1111/j.2153-3490.1968.tb00364.x.

Cotton, W. R., and Coauthors, 2003: RAMS 2001: Current status and future directions. *Meteor. Atmos. Phys.,* **82,** 5–29, doi:10.1007/s00703-001-0584-9.

Cui, Z., K. S. Carslaw, and A. M. Blyth, 2011: The coupled effect of mid-tropospheric moisture and aerosol abundance on deep convective cloud dynamics and microphysics. *Atmosphere,* **2,** 222–241, doi:10.3390/atmos2030222.

Davies-Jones, R., 2002: Linear and nonlinear propagation of supercell storms. *J. Atmos. Sci.,* **59,** 3178–3205, doi:10.1175/1520-0469(2003)059<3178:LANPOS>2.0.CO;2.

DeMott, P. J., and Coauthors, 2010: Predicting global atmospheric ice nuclei distributions and their impacts on climate. *Proc. Natl. Acad. Sci. USA,* **107,** 11 217–11 222, doi:10.1073/pnas.0910818107.

Droegemeier, K. K., S. M. Lazarus, and R. Davies-Jones, 1993: The influence of helicity on numerically simulated convective storms. *Mon. Wea. Rev.,* **121,** 2005–2029, doi:10.1175/1520-0493(1993)121<2005:TIOHON>2.0.CO;2.

Ekman, A. M. L., A. Engström, and C. Wang, 2007: The effect of aerosol composition and concentration on the development and anvil properties of a continental deep convective cloud. *Quart. J. Roy. Meteor. Soc.,* **133,** 1439–1452, doi:10.1002/qj.108.

Emanuel, K. A., 1994: *Atmospheric Convection.* Oxford University Press, 580 pp.

Feingold, G., and A. J. Heymsfield, 1992: Parameterizations of condensational growth of droplets for use in general circulation models. *J. Atmos. Sci.,* **49,** 2325–2342, doi:10.1175/1520-0469(1992)049<2325:POCGOD>2.0.CO;2.

Fovell, R. G., and P.-H. Tan, 1998: The temporal behavior of numerically simulated multicell-type storms. Part II: The convective cell life cycle and cell regeneration. *Mon. Wea. Rev.,* **126,** 551–577, doi:10.1175/1520-0493(1998)126<0551:TTBONS>2.0.CO;2.

Gilmore, M. S., and L. J. Wicker, 1998: The influence of midtropospheric dryness on supercell morphology and evolution. *Mon. Wea. Rev.,* **126,** 943–958, doi:10.1175/1520-0493(1998)126<0943:TIOMDO>2.0.CO;2.

Grant, L. D., and S. C. van den Heever, 2014: Microphysical and dynamical characteristics of low-precipitation and classic supercells. *J. Atmos. Sci.,* **71,** 2604–2624, doi:10.1175/JAS-D-13-0261.1.

James, R. P., and P. M. Markowski, 2010: A numerical investigation of the effects of dry air aloft on deep convection. *Mon. Wea. Rev.,* **138,** 140–161, doi:10.1175/2009MWR3018.1.

Johnson, R. H., and P. J. Hamilton, 1988: The relationship of surface pressure features to the precipitation and airflow structure of an intense midlatitude squall line. *Mon. Wea. Rev.,* **116,** 1444–1473, doi:10.1175/1520-0493(1988)116<1444:TROSPF>2.0.CO;2.

Khain, A., and B. Lynn, 2009: Simulation of a supercell storm in clean and dirty atmosphere using weather research and forecast model with spectral bin microphysics. *J. Geophys. Res.,* **114,** D19209, doi:10.1029/2009JD011827.

——, D. Rosenfeld, and A. Pokrovsky, 2005: Aerosol impact on the dynamics and microphysics of deep convective clouds. *Quart. J. Roy. Meteor. Soc.,* **131,** 2639–2663, doi:10.1256/qj.04.62.

——, N. BenMoshe, and A. Pokrovsky, 2008: Factors determining the impact of aerosols on surface precipitation from clouds: An attempt at classification. *J. Atmos. Sci.,* **65,** 1721–1748, doi:10.1175/2007JAS2515.1.

——, D. Rosenfeld, A. Pokrovsky, U. Blahak, and A. Ryzhkov, 2011: The role of CCN in precipitation and hail in a midlatitude storm as seen in simulations using a spectral (bin) microphysics model in a 2D dynamic frame. *Atmos. Res.,* **99,** 129–146, doi:10.1016/j.atmosres.2010.09.015.

Khairoutdinov, M., and D. Randall, 2006: High-resolution simulation of shallow-to-deep convection transition over land. *J. Atmos. Sci.,* **63,** 3421–3436, doi:10.1175/JAS3810.1.

Klemp, J. B., and R. B. Wilhelmson, 1978: The simulation of three-dimensional convective storm dynamics. *J. Atmos. Sci.,* **35,** 1070–1096, doi:10.1175/1520-0469(1978)035<1070:TSOTDC>2.0.CO;2.

Kuang, Z., and C. S. Bretherton, 2006: A mass-flux scheme view of a high-resolution simulation of a transition from shallow to deep cumulus convection. *J. Atmos. Sci.,* **63,** 1895–1909, doi:10.1175/JAS3723.1.

Lee, S. S., 2011: Dependence of aerosol-precipitation interactions on humidity in a multiple-cloud system. *Atmos. Chem. Phys.,* **11,** 2179–2196, doi:10.5194/acp-11-2179-2011.

——, L. J. Donner, V. T. J. Phillips, and Y. Ming, 2008: Examination of aerosol effects on precipitation in deep convective clouds during the 1997 ARM summer experiment. *Quart. J. Roy. Meteor. Soc.,* **134,** 1201–1220, doi:10.1002/qj.287.

Lim, K.-S. S., S.-Y. Hong, S. S. Yum, J. Dudhia, and J. B. Klemp, 2011: Aerosol effects on the development of a supercell storm in a double-moment bulk-cloud microphysics scheme. *J. Geophys. Res.,* **116,** D02204, doi:10.1029/2010JD014128.

Lin, Y.-L., R. L. Deal, and M. S. Kulie, 1998: Mechanisms of cell regeneration, development, and propagation within a two-dimensional multicell storm. *J. Atmos. Sci.,* **55,** 1867–1886, doi:10.1175/1520-0469(1998)055<1867:MOCRDA>2.0.CO;2.

Loftus, A. M., and W. R. Cotton, 2014: Examination of CCN impacts on hail in a simulated supercell storm with triple-moment hail bulk microphysics. *Atmos. Res.,* **147–148,** 183–204, doi:10.1016/j.atmosres.2014.04.017.

May, P. T., V. N. Bringi, and M. Thurai, 2011: Do we observe aerosol impacts on DSDs in strongly forced tropical thunderstorms? *J. Atmos. Sci.,* **68,** 1902–1910, doi:10.1175/2011JAS3617.1.

Meyers, M. P., R. L. Walko, J. Y. Harrington, and W. R. Cotton, 1997: New RAMS cloud microphysics parameterization. Part II: The two-moment scheme. *Atmos. Res.,* **45,** 3–39, doi:10.1016/S0169-8095(97)00018-5.

Morrison, H., 2012: On the robustness of aerosol effects on an idealized supercell storm simulated with a cloud system-resolving model. *Atmos. Chem. Phys.,* **12,** 7689–7705, doi:10.5194/acp-12-7689-2012.

Prospero, J. M., P. Ginoux, O. Torres, S. E. Nicholson, and T. E. Gill, 2002: Environmental characterization of global sources of atmospheric soil dust identified with the NIMBUS 7 Total Ozone Mapping Spectrometer (TOMS) absorbing aerosol product. *Rev. Geophys.,* **40,** 1002, doi:10.1029/2000RG000095.

Ridout, J. A., 2002: Sensitivity of tropical Pacific convection to dry layers at mid- to upper levels: Simulation and parameterization tests. *J. Atmos. Sci.,* **59,** 3362–3381, doi:10.1175/1520-0469(2002)059<3362:SOTPCT>2.0.CO;2.

Rotunno, R., and J. B. Klemp, 1982: The influence of the shear-induced pressure gradient on thunderstorm motion. *Mon. Wea. Rev.,* **110,** 136–151, doi:10.1175/1520-0493(1982)110<0136:TIOTSI>2.0.CO;2.

Saleeby, S. M., and W. R. Cotton, 2004: A large-droplet mode and prognostic number concentration of cloud droplets in the Colorado State University Regional Atmospheric Modeling System (RAMS). Part I: Module descriptions and supercell test simulations. *J. Appl. Meteor.,* **43,** 182–195, doi:10.1175/1520-0450(2004)043<0182:ALMAPN>2.0.CO;2.

——, and ——, 2008: A binned approach to cloud-droplet riming implemented in a bulk microphysics model. *J. Appl. Meteor. Climatol.,* **47,** 694–703, doi:10.1175/2007JAMC1664.1.

——, and S. C. van den Heever, 2013: Developments in the CSU-RAMS aerosol model: Emissions, nucleation, regeneration, deposition, and radiation. *J. Appl. Meteor. Climatol.,* **52,** 2601–2622, doi:10.1175/JAMC-D-12-0312.1.

——, W. Berg, S. van den Heever, and T. L'Ecuyer, 2010: Impact of cloud-nucleating aerosols in cloud-resolving model simulations of warm-rain precipitation in the East China Sea. *J. Atmos. Sci.,* **67,** 3916–3930, doi:10.1175/2010JAS3528.1.

Seifert, A., and K. D. Beheng, 2006: A two-moment cloud microphysics parameterization for mixed-phase clouds. Part 2: Maritime vs. continental deep convective storms. *Meteor. Atmos. Phys.,* **92,** 67–82, doi:10.1007/s00703-005-0113-3.

Seigel, R. B., S. C. van den Heever, and S. M. Saleeby, 2013: Mineral dust indirect effects and cloud radiative feedbacks of a simulated idealized nocturnal squall line. *Atmos. Chem. Phys.,* **13,** 4467–4485, doi:10.5194/acp-13-4467-2013.

Smagorinsky, J., 1963: General circulation experiments with the primitive equations. I. The basic experiment. *Mon. Wea. Rev.,* **91,** 99–164, doi:10.1175/1520-0493(1963)091<0099:GCEWTP>2.3.CO;2.

Storer, R. L., and S. C. van den Heever, 2013: Microphysical processes evident in aerosol forcing of tropical deep convective clouds. *J. Atmos. Sci.,* **70,** 430–446, doi:10.1175/JAS-D-12-076.1.

——, ——, and G. L. Stephens, 2010: Modeling aerosol impacts on convective storms in different environments. *J. Atmos. Sci.,* **67,** 3904–3915, doi:10.1175/2010JAS3363.1.

Tao, W.-K., X. Li, A. Khain, T. Matsui, S. Lang, and J. Simpson, 2007: Role of atmospheric aerosol concentration on deep convective precipitation: Cloud-resolving model simulations. *J. Geophys. Res.,* **112,** D24S18, doi:10.1029/2007JD008728.

——, J.-P. Chen, Z. Li, C. Wang, and C. Zhang, 2012: Impact of aerosols on convective clouds and precipitation. *Rev. Geophys.,* **50,** RG2001, doi:10.1029/2011RG000369.

Thorpe, A. J., and M. J. Miller, 1978: Numerical simulations showing the role of the downdraught in cumulonimbus motion and splitting. *Quart. J. Roy. Meteor. Soc.,* **104,** 873–893, doi:10.1002/qj.49710444203.

——, ——, and M. W. Moncrieff, 1982: Two-dimensional convection in non-constant shear: A model of mid-latitude squall lines. *Quart. J. Roy. Meteor. Soc.,* **108,** 739–762, doi:10.1002/qj.49710845802.

van den Heever, S. C., and W. R. Cotton, 2007: Urban aerosol impacts on downwind convective storms. *J. Appl. Meteor. Climatol.,* **46,** 828–850, doi:10.1175/JAM2492.1.

——, G. G. Carrió, W. R. Cotton, P. J. DeMott, and A. J. Prenni, 2006: Impacts of nucleating aerosol on Florida storms. Part I: Mesoscale simulations. *J. Atmos. Sci.,* **63,** 1752–1775, doi:10.1175/JAS3713.1.

Walko, R. L., W. R. Cotton, M. P. Meyers, and J. Y. Harrington, 1995: New RAMS cloud microphysics parameterization. Part I: The single-moment scheme. *Atmos. Res.,* **38,** 29–62, doi:10.1016/0169-8095(94)00087-T.

Weisman, M. L., and J. B. Klemp, 1982: The dependence of numerically simulated convective storms on vertical wind shear and buoyancy. *Mon. Wea. Rev.,* **110,** 504–520, doi:10.1175/1520-0493(1982)110<0504:TDONSC>2.0.CO;2.

——, and ——, 1984: The structure and classification of numerically simulated convective storms in directionally varying wind shears. *Mon. Wea. Rev.,* **112,** 2479–2498, doi:10.1175/1520-0493(1984)112<2479:TSACON>2.0.CO;2.